






# Supplementary Loop in BESS Control Scheme for SSO Mitigation in DFIG-Based Wind Farms

R. Moreno-Sánchez , N. Visairo-Cruz , *Member, IEEE*, C. A. Núñez-Gutiérrez , *Member, IEEE*, J. Hernández-Ramírez , and J. Segundo-Ramírez , *Member, IEEE*

**Abstract**—This paper addresses the problem of Subsynchronous Oscillations (SSO) in a Doubly Fed Induction Generator (DFIG) wind farm originated by its interaction with a series-compensated transmission line. Given its relevance in the power system, several solutions and analysis methods have been utilized to tackle this issue. This article proposes an innovative function for a Battery Energy Storage System (BESS) in mitigating SSO without compromising its primary functions. To achieve this aim, the article explains the origin of SSO and outlines how incorporating a BESS can effectively ease it. To evaluate the feasibility of this proposal, we conduct extensive simulations on a power system integrating energy-distributed resources from DFIG-based wind farms, employing a BESS to compensate for SSO induced by a series-compensated transmission line. The results confirm that BESS is highly effective in reducing or even eliminating SSO.

Link to graphical and video abstracts, and to code: <https://latam.ieceer9.org/index.php/transactions/article/view/9029>

**Index Terms**—Doubly Fed Induction Generator (DFIG), Battery Energy Storage System (BESS), Modal Analysis, Subsynchronous Resonance (SSR), Subsynchronous Oscillations (SSO), wind farm, DFIG.

## I. INTRODUCTION

In recent decades, wind energy utilization has surged, particularly with DFIG-based wind farms, leading to substantial growth in this sector. However, challenges like Subsynchronous Interactions (SSIs) have emerged, necessitating a thorough understanding of their origins for effective resolution [1]–[8]. Various analytical techniques have been employed to study the instability caused by Subsynchronous Oscillations (SSO), including impedance equivalent models, Bode plots, and Nyquist plots [9]–[18].

This paper implements the developed methodology proposed in [19] and also addresses the mitigation and analysis of the SSO. For instance, if SSO arises from Subsynchronous Control Interactions (SSCI), adjusting power electronic controllers may offer the most promising solution [20]. However, it is noteworthy that investigating the root cause of SSO is

The associate editor coordinating the review of this manuscript and approving it for publication was Pedro Moura (*Corresponding author: Roberto Moreno*).

The authors would like to thank the scholarship CONACyT 485936, the projects SEP-CONACyT A1-S-29705, and CF 2019/1311344.

R. Moreno-Sánchez, N. Visairo-Cruz, C. A. Núñez-Gutiérrez, J. Hernández-Ramírez, and J. Segundo-Ramírez are with the Universidad Autónoma de San Luis Potosí, San Luis Potosí, México (e-mails: roberto.mor.san@hotmail.com, nvisairoc@uaslp.mx, calberto@uaslp.mx, jarmonyhr@gmail.com, and juan.segundo@uaslp.mx).

not common. As an example, in [21] the authors describe the basic characteristic of the phenomenon, and based on it, it is assumed that the subsynchronous oscillations are due to Subsynchronous Resonance (SSR).

According to previous research [22]–[24], it is proven that, incorporating Battery Energy Storage Systems (BESS) in modern power systems or microgrids can significantly enhance the power management and system stability. For instance, combining a BESS with a Static Synchronous Compensator (STATCOM) offers superior flexibility and improved voltage and power management capabilities [25]–[27].

Nevertheless, there remains a need for extensive research on mitigating SSO using BESS as a multifunctional device in Wind Energy Conversion Systems (WECS). For example, in [28] the author mitigates the SSO by a BESS (without showing the analysis of the origin of the oscillations), this work focuses on the compensation of active power oscillation produced by the SSO. On the other hand, in [20] the authors achieve maximum damping characteristics by optimizing the proportional and derivative gains of the back-to-back controllers of the DFIG. Those scenarios are implemented and compared with the proposal in the following sections.

The structure of this paper is as follows: Section II provides background information, while Section III discusses the system under study, BESS controller, and presents the proposal statement. Section IV thoroughly examines the system performance, followed by small-signal stability analysis in Section V. Section VI outlines the proposed mitigation scheme, and finally, Section VII presents the conclusions drawn from this study.

## II. BACKGROUND

Subsynchronous interaction describes the oscillation of a system with frequencies below the synchronous frequency [16]. The phenomena are classified as SSR, SSCI, and Subsynchronous Torsional Interaction (SSTI).

SSR can be attributed to three phenomena: Induction Generator Effect (IGE), Torque Amplification (TA), and Torsional Interaction (TI) [29]. IGE is an electrical phenomenon; the system will experience negative damping if the rotor resistance, as viewed from the stator terminals, is greater than the stator and power system resistances. TA refers to the interaction between an electromechanical system and a series-compensated transmission line and this can be expressed as:

$$f_m = f_o \pm f_{er} \quad (1)$$

where (1) defines the component of frequency induced ( $f_m$ ) in the generator due to the natural frequency of the transmission line ( $f_{er}$ ).  $f_o$  represents the rotor electrical frequency. TI refers to the interaction between the mechanical system of the turbine-generator and an electrical network that has been series-compensated [16], [29], [30]; the expression:

$$f_{en} = f_o \pm f_n \quad (2)$$

defines the component of frequency rendered ( $f_{en}$ ) to the terminals of the generator due to the natural frequency of the shaft system ( $f_n$ ) [16], [29], [30].

SSTI refers to oscillations below the system frequency produced when the natural frequency of the mechanical systems interacts with the negative damping of the controller of the power electronics [16]. SSCI refers to oscillation below the system frequency produced when the natural frequency of the network interacts with the power electronic control system [16].

### III. PROPOSAL STATEMENT

The study framework focuses on a BESS integrated with a wind farm. Its primary role is managing active power sent to the grid, either absorbing or supplying energy. Embedded within this function is the proposal to mitigate SSO. In this context, quantifying the impact of active power control and the proposed mitigation method is crucial. So, this section outlines the key features of the BESS and the implemented methodology.

#### A. System Model

The system under analysis is shown in Fig. 1. The parameters of the wind, drive train, induction generator, back-to-back converter and its PI gains, Voltage Source Converter (VSC) for the BESS and its PI gains, transmission line, and its mathematical models are obtained from [9], [19], [31]. In this context, it is considered the following:

- The BESS has the task of ensuring the transmission of 1 pu of active power to the electrical network.
- It is considered an ideal DC source for the BESS.
- For analysis purposes, the series capacitive compensation ( $K_{cs}$ ) is considered from 0% to 100% [32], [33].

Besides the statements above, this section sets up the control for BESS. Fig. 2 shows the decoupled PI control scheme of the BESS in the synchronous reference frame [34], where  $P$  and  $Q$  are the active and reactive powers, and the suffix *bess*, *ref*, and *dfig* correspond to the BESS, reference, and wind farm quantities, respectively,  $\omega_b$  is the base frequency and  $L_b$  is the BESS inductance. Those quantities are measured in the bus B1 in  $dq$  synchronous reference frame. The voltage of Bus B1 is controlled through the DFIG scheme, in this scenario  $i_{qb\_ref} = 0$ . The voltage balance across the impedance for the BESS is:

$$v_{B1} = v_{bs} + R_b i_b + L_b \frac{di_b}{dt} \quad (3)$$

The transformation of (3) into a  $dq$  synchronous oriented reference frame [5], [16], [19], [35], as follows:

$$\frac{L_b}{\omega_b} \frac{d}{dt} \begin{bmatrix} i_{db} \\ i_{qb} \end{bmatrix} = \begin{bmatrix} v_{dB1} \\ v_{qB1} \end{bmatrix} - \begin{bmatrix} v_{db} \\ v_{qb} \end{bmatrix} - R_b \begin{bmatrix} i_{db} \\ i_{qb} \end{bmatrix} - \omega_b L_b \begin{bmatrix} -i_{qb} \\ +i_{db} \end{bmatrix} \quad (4)$$

where  $i_{db}$  and  $i_{qb}$  are the BESS currents,  $v_{db}$  and  $v_{qb}$  are the VSC voltage. Equation (4) includes coupled terms, the reference voltages with compensation terms are:

$$\begin{bmatrix} v_{db}^* \\ v_{qb}^* \end{bmatrix} = \begin{bmatrix} v_{dB1} \\ v_{qB1} \end{bmatrix} + \omega_b L_b \begin{bmatrix} +i_{qb} \\ -i_{db} \end{bmatrix} - \begin{bmatrix} v_{db}' \\ v_{qb}' \end{bmatrix} \quad (5)$$

where the symbol \* refers to a reference voltages and ' refers to the control signals.

#### B. Methodology

The active power control of the BESS and the proposed mitigation control must be able to operate without conflict between them. Considering the previous and the aim of the research, the analysis methodology outlined can be summarized as follows:

- Dynamic simulation is employed to determine the series compensation limit where the wind farm exhibits SSO.
- Modal Impedance (MI) analysis is applied to find the frequency of resonance and to establish if the resonance is "induced or rendered".
- Subsequently, the Selective Modal Analysis (SMA) identifies critical modes and the physical components contributing to SSI.
- Applying the SMA tools, a parametric analysis is performed to show the misinterpretation of the results when an integral analysis is omitted.
- Building on SMA findings, a targeted solution is proposed due to the origin of the oscillation can be established.

Consequently, the contributions are twofold:

- The methodology implementation helps to identify the phenomenon and the elements involved in SSI leading to the correct interpretation of the results.
- The proposed mitigation scheme mitigates the SSO at any level of series compensation; improving the case with the active power control and the case with the parametric analysis.

The objective of this Proposed Mitigation Scheme (PMS) is to isolate the currents that generate SSO by separating the two system elements interacting at low frequencies. Notably, the simplicity of the PMS allows other control schemes to function concurrently. Furthermore, to mitigate the SSI phenomenon, the PMS requires finite energy, only during the initial transient phase.

On the other hand, the results are obtained by simulating the system in ODE's of MATLAB/Simulink, validated by PSCAD. The setup information of the dynamic equations in ODE's can be found in detail in [31].

### IV. PERFORMANCE OF THE SYSTEM

#### A. Dynamic Simulation

Dynamic simulations (performed in MATLAB/Simulink 2018b) investigate the series compensation limit that the

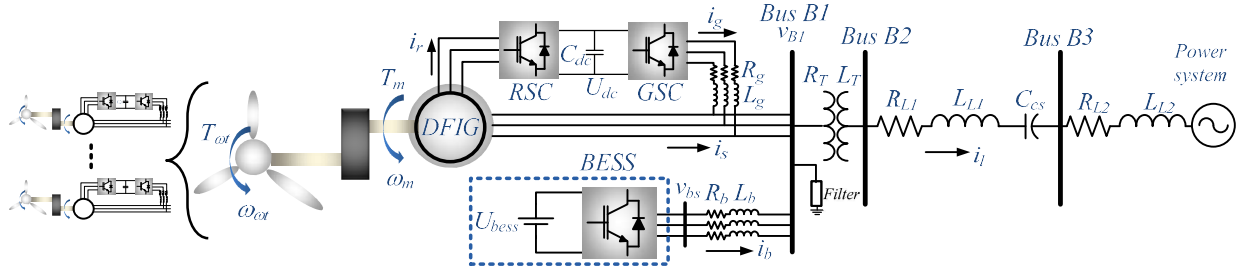


Fig. 1. BESS integration into the DFIG-based wind farm [19].

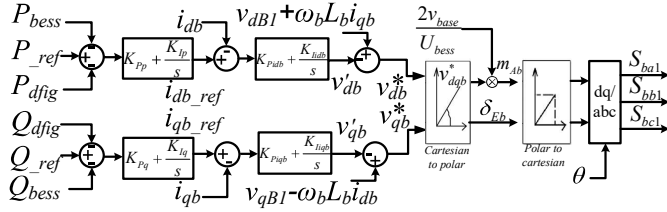


Fig. 2. Active power control of the BESS [34].

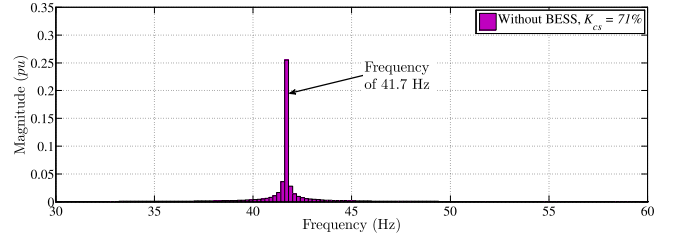


Fig. 4. FFT of the electric torque,  $K_{cs} = 71\%$ , without BESS; Fig. 3.

system can handle before an SSO arises. To apply the PMS, it is essential to understand the Active Power Control (APC) capabilities. Two scenarios are examined: the wind farm without the BESS and the wind farm with the APC in the BESS, both near the compensation limit.

When the system remains in the steady state a change of series compensation can be applied, in this context, Fig. 3 shows simulations near the resonance zone, starting with  $K_{cs} = 10\%$  without BESS, the system remains stable up to  $K_{cs} = 70\%$  but becomes unstable at  $K_{cs} = 71\%$ , establishing the compensation limit at 71%. However, with APC in the BESS, the system remains stable at  $K_{cs} = 71\%$ . The limit of compensation that the APC can handle before SSO is analyzed in Section V.A.

With this information, the SSO frequency shows a dominant magnitude of 41.7 Hz in the electric torque (Fig 4). This frequency results from the interaction between two subsystems, which is paramount to the research objectives. SSCI and SSTI can be assessed using small-signal analysis, while SSR can be evaluated using MI analysis [36]. Identifying the origin of the phenomenon is essential before establishing a targeted solution.

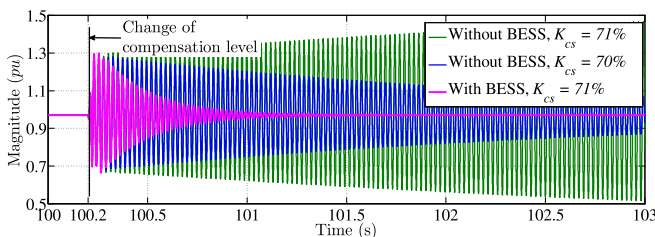


Fig. 3. Electric torque, the system under three different scenarios.

### B. Steady-State Equivalent Circuit

The equivalent circuit is used for MI analysis, which combines driving point impedance and eigenvalue analysis to verify the natural frequencies ( $f_{er}$ ) of electrical elements in the power system. Fig. 5 shows the steady-state equivalent circuit of the system, where  $S_{ssr}$  is the rotor slip,  $R_{eq}^{S_{ssr}}$  is the SSR equivalent rotor resistance,  $X_{lr}$  is the rotor leakage impedance,  $X_m$  is the mutual impedance,  $R_s$  is the stator resistance,  $X_{ls}$  is the stator leakage impedance, the subscript  $g$  refers to GSC impedance, the subscript  $b$  refers to the BESS impedance, and the subscript  $tot$  refers to the transmission line and transformer impedance.

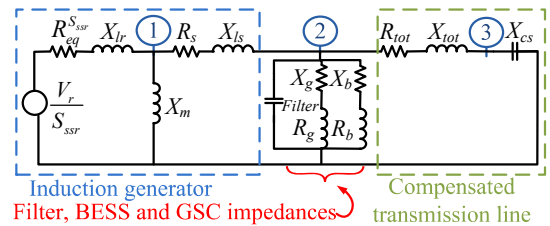


Fig. 5. Equivalent electric circuit of the wind farm.

Considering the compensation limit, MI analysis, and equation (1), Fig. 6 shows frequency versus series compensation level. The compensation limit (magenta line) is at 71%. The frequency component  $f_{er}$  (blue line) intersects the compensation limit at 19.53 Hz, and the induced component frequency is 41.67 Hz. For the induction generator, the rotor's electrical speed is  $f_o = f_s \times Slip$ , with  $f_s$  as the synchronous frequency and  $Slip = 1.02$  [15], [19].

The dynamic simulation shows an SSO frequency of 41.7 Hz, and the MI analysis indicates an induced frequency of 41.67 Hz at the compensation limit. Thus, the SSO is due to the induced component  $f_m$ . SSCI, IGE, TI, and TA can be

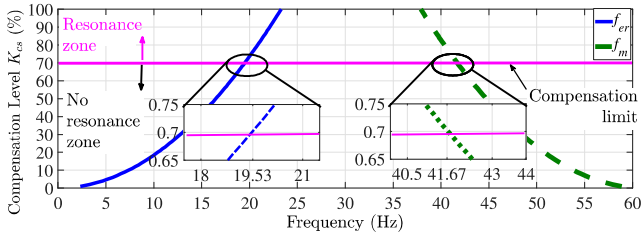


Fig. 6. Subsynchronous resonance frequency versus series compensation level.

the origin of the SSO as they all involve series compensation topology. The next step is identifying the frequencies of the modes of interest and the interacting physical elements causing SSI.

## V. SMALL-SIGNAL STABILITY ANALYSIS

The system dynamic equations, a set of nonlinear ODEs, are simulated in MATLAB/Simulink 2018b. To apply SMA, the system is linearized using MATLAB's *fsolve* function to compute the steady state and Jacobian matrix. This analysis compares the system without BESS to one with APC in the BESS, including a parametric variation case study. Based on these results, the proposed scheme is developed in the next section.

### A. Eigenvalue Analysis and Participation Factors

This analysis investigates the two elements involved in the SSO phenomenon; the system enhancement is quantified. The following cases are proposed:

- Base Case: series compensation of 10%, 70%, and 71% without the BESS.
- Case A: series compensation of 10%, 70%, 71%, 77.7%, and 77.8% with the BESS with APC.

Following the procedure in [19], mode 12/13 (complex conjugates) is identified as the critical mode that causes system instability. Table I shows the characteristics of this critical mode for the Base Case and Case A.

TABLE I  
MODES 12/13, CRITICAL MODE

Cases	$K_{cs}(\%)$	$\sigma$	$f$ (Hz)	$\zeta$	D. State/PF
Base	10	-18.12	38.14	$7.538 \times 10^{-3}$	$\Delta i_{dr}$ 7.31
Case	70	-0.1696	41.68	$6.477 \times 10^{-4}$	$\Delta i_{dr}$ 9.03
	71	0.4385	41.67	$-1.675 \times 10^{-3}$	$\Delta i_{dr}$ 8.81
	10	-19.75	38.26	$8.187 \times 10^{-2}$	$\Delta i_{dr}$ 7.50
Case A	70	-4.701	41.76	$1.791 \times 10^{-2}$	$\Delta i_{dr}$ 10.6
	71	-4.038	41.76	$1.539 \times 10^{-2}$	$\Delta i_{dr}$ 10.3
	77.7	-0.0189	41.67	$7.234 \times 10^{-5}$	$\Delta i_{dr}$ 8.59
	77.8	0.03604	41.67	$-1.376 \times 10^{-4}$	$\Delta i_{dr}$ 8.57

$\sigma \rightarrow$  real eigenvalue,  $f \rightarrow$  oscillation frequency,  $\zeta \rightarrow$  damping ratio.

The study evaluates the stability of a system with the BESS employing the APC and the system without the BESS. In the absence of the BESS, the system stability is tested at various compensation levels, indicating instability at 71%. However, with BESS employing the APC, the stability improves significantly until  $K_{cs} = 77.7\%$ , shown by their eigenvalues and damping factor. According to Table I, the rotor current is identified as the critical state variable in the unstable mode,

highlighting this mode showing SSO despite BESS integration after a compensation level of  $K_{cs} = 77.8\%$ . Furthermore, the instability is found at 41.67 Hz for both cases.

Given these findings, it is imperative to investigate the interaction of the modes involved in the SSO condition before proposing a mitigation strategy. According to the state of the art, the modes involved in SSO condition are related to the mechanical and electrical transferring-energy-process; i.e., if two modes are close enough SSO condition can occur [29], in this context according to Fig. 7 the electromechanical mode and subsynchronous induced mode are getting close. Fig. 7 also shows the evolution of mechanical mode. The modes shown in Fig. 7 are compared, the modes without the BESS and those with the BESS playing the APC. Using the analysis from Section IV-B supersynchronous electrical mode (*SupSR Elec Mode*) and the subsynchronous electrical mode (*SSR Elec Mode*) are computed, illustrated in Fig. 7a, those are used to identify the induced modes for the small-signal analysis [19]; corresponding to modes 8/9 and 10/11. The electromechanical mode is identified as mode 12/13. The mechanical mode is identified as mode 16/17, with  $\lambda_{16/17} = -63.9 \pm j11.7$  for  $K_{cs}$  from 0% to 100%.

The modes that are getting closer are the subsynchronous induced mode and the electromechanical mode, those modes produce the SSO. In conclusion, the series capacitor transfers energy to the electromechanical system by inducing subsynchronous components to the induction generator. Those are the elements that are interchanging energy on the SSO condition. In conclusion, according to the definitions of SSI, torque amplification is identified as the origin of the SSO.

TABLE II  
PARTICIPATION FACTORS WITH  $K_{cs} = 10\%$

Modes	Variable	Case without BESS (%)	Case with the APC (%)
$\lambda_{8/9}$	$\Delta i_{qs}$	19.9	19.8
	$\Delta i_{ds}$	26.6	26.8
	$\Delta i_{qr}$	17.8	17.7
	$\Delta i_{dr}$	24.8	24.9
	$\Delta V_{dcs}$	5.1	5.1
	$\Delta V_{qcs}$	5.1	5.2
$\lambda_{10/11}$	$\Delta i_{qs}$	20.2	20.1
	$\Delta i_{ds}$	30.4	30.5
	$\Delta i_{qr}$	18.2	18.1
	$\Delta i_{dr}$	28.7	28.8
$\lambda_{12/13}$	$\Delta i_{qs}$	8.9	8.6
	$\Delta i_{ds}$	38.2	38.5
	$\Delta i_{qr}$	8.3	8.1
	$\Delta i_{dr}$	41.4	41.6
$\lambda_{16/17}$	$\Delta i_{qs}$	5.5	5.6
	$\Delta i_{ds}$	1.4	1.6
	$\Delta i_{qr}$	6.9	7.1
	$\Delta i_{dr}$	1.5	1.8
	$\Delta X_1$	41.4	40.1
	$\Delta X_2$	42.4	42.0

← Maximum value

Up to this point, the modes involved in the SSO have been identified and, consequently, the phenomenon has been identified. Moreover, according to Table II the rotor and stator currents are the state variables with more participation, their contribution to the dynamics of the resonance condition is much higher than the rest of the state variables. Now, as a study case, the damping can be improved even more with



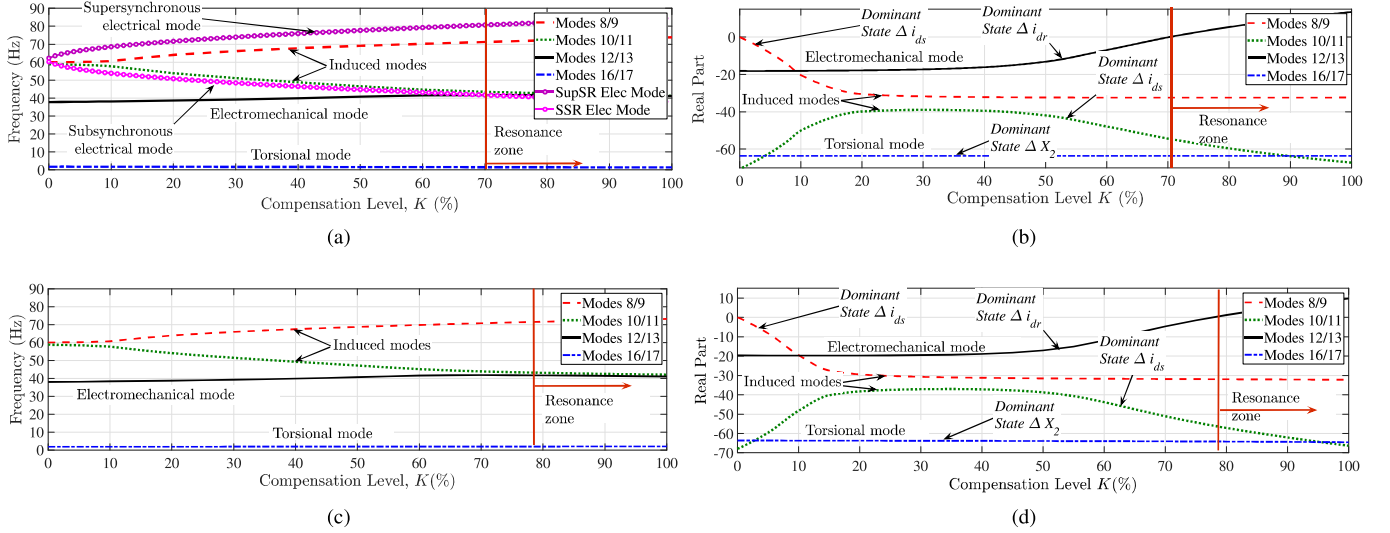


Fig. 7. Evolution of the main eigenvalues, without the BESS and the BESS with APC. (a) Evolution of the frequency without the BESS. (b) Evolution of the real part without the BESS. (c) Evolution of the frequency with the BESS with APC. (d) Evolution of the real part with the BESS with APC.

the BESS applying only the APC. To achieve that, sensitivity analysis is required, and based on it, a mathematical expression is developed to figure out which parameter can be modified.

### B. Eigenvalue Sensitivity

According to [15], the mathematical definition of eigenvalue sensitivity is:

$$\frac{\partial \lambda_i}{\partial a_{k,j}} = \psi_{i,k} \phi_{j,i} \quad (6)$$

where  $i$  is the eigenvalue of interest,  $a_{k,j}$  is the element of the Jacobian matrix of the  $k$ -th row and  $j$ -th column. It is necessary to improve the critical eigenvalue by shifting it to the left in the  $s$ -plane. In this case, it is required to compute the sensitivity matrix for such mode ( $S^{12/13}$ ), but the more significant sensitivity value and its linearized state of the Jacobian matrix ( $A = J(X_0) = \frac{\partial f}{\partial x} |_{x=X_0}$ ) is analyzed.

The matrix  $S^{12/13}$  is shown in Fig. 8; a common level of series compensation of 10% is set. Here, the maximum sensitivity of the eigenvalues can be found in the 7th row and the 7th column;  $S_{7,7}^{12/13}$ . The equation (6) can be re-written as:

$$\frac{\Delta \lambda_{12/13}}{\Delta a_{7,7}} \approx S_{7,7}^{12/13} \quad (7)$$

To estimate the motion of the eigenvalue  $\lambda_{12/13}$ , a general expression can be used. Taking  $\Delta a_{7,7} \approx a_{7,7}^n - a_{7,7}^0$ , where  $a_{7,7}$  is the element on 7th row and 7th column of the Jacobian matrix, the power 0 is the current value and the power  $n$  is the expected value. In this sense, from (7) the next statement is deduced:

$$\lambda_{12/13}^n \approx \lambda_{12/13}^0 + S_{7,7}^{12/13} (a_{7,7}^n - a_{7,7}^0) \quad (8)$$

To improve the stability,  $\lambda_{12/13}^n$  must be moved to the left side of the  $s$ -plane. Considering  $\lambda_{12/13}^0 = -19.749 \pm j240.408$  and  $S_{7,7}^{12/13} = 7.474 + j0.6155$ . When computing  $(a_{7,7}^n - a_{7,7}^0)$ ,

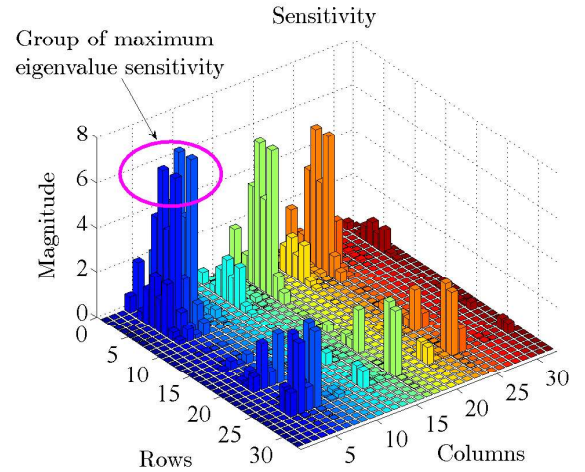


Fig. 8. Sensitivity matrix,  $S^{12/13}$ , with  $K_{cs} = 10\%$ .

the result must be negative. Taking into consideration the differential equations of the system, the partial derivative of  $a_{7,7}$  of the  $A$  matrix is:

$$a_{7,7} = D \left( R_r L_s - L_s \frac{\partial v_{dr}}{\partial i_{dr}} \right) \quad (9)$$

where all the quantities in  $a_{7,7}$  are in  $pu$ ,  $D = \omega_b / (L_m^2 - L_r L_s)$  and the partial derivative  $\frac{\partial v_{dr}}{\partial i_{dr}}$  is computed numerically through MatLab/Simulink.

Based on (8) and (9), the condition  $(a_{7,7}^n - a_{7,7}^0) < 0$  must be fulfilled to  $\lambda_{12/13}$  moves toward the left side. As a case of study, the parameters in (9) are modified, as the rotor leakage inductance ( $L_{lr}$ ) and the proportional gain  $K_{Pidr}$  from the rotor voltage controller.

Fig. 9 displays the eigenvalue of  $\lambda_{12/13}$ ; real part versus compensation level. According to Fig. 9, the stability of the system can be improved by parametric variation. The

eigenvalue turns positive at 88% when the inductance  $L_{lr}$  is adjusted. When  $K_{Pidr}$  is modified, the system can alleviate damping during SSO. This finding underscores that enhancing system stability, observed during SSO by adjusting control gain parameters, does not necessarily indicate a control-related origin [37]. On the other side, stability is improved through parametric variation, however, a resonance condition persists under a specific level of series compensation.

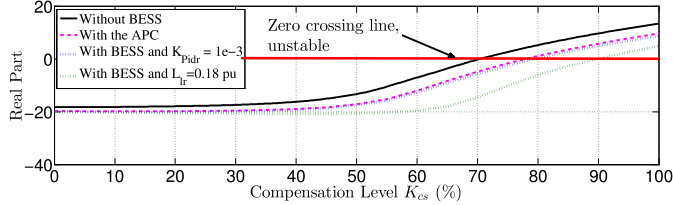


Fig. 9. Real part of the electromechanical mode with parameters variation.

## VI. DESIGN PRINCIPLES OF PROPOSED MITIGATING SCHEME

In this section, we develop the PMS and conduct a SMA to showcase the scope of our proposal. The performance of the PMS is then compared with a scenario involving BESS with only APC. The objective is to mitigate or eliminate subsynchronous resonance conditions at any level of series compensation.

### A. Designing the Scheme

According to the previous small-signal stability analysis, the stator and rotor currents are the means by which the energy is transferred between the two elements under TA. According to Fig. 10, the stator currents are related to the subsynchronous natural frequency ( $f_{er}$ ) by:

$$i_s = i_l - i_g - i_b \quad (10)$$

where  $i_l$ ,  $i_g$ ,  $i_s$ , and  $i_b$  are the currents of the line, back-to-back converter, induction generator, and the BESS, respectively. Under a transient (with a series compensation of  $K_{cs} = 71\%$ ), the electrical network shows a subsynchronous natural frequency of  $f_{er} = 19.53$  Hz. This component is induced into the generator through the stator currents according to (10) and then through the rotor currents; a simplification of the induction generator [19], [31] can be used to show the relation between those currents as follows:

$$\begin{aligned} \frac{1}{\omega_b} \frac{di_{dr}}{dt} &= -(v_{ds} - R_s i_{ds} + \omega_s \psi_{qs}) L_m / L_r L_s \alpha \\ &\quad + (v_{dr} - R_r i_{dr} + \omega_s \psi_{qr}) / L_r \alpha \\ \frac{1}{\omega_b} \frac{di_{qr}}{dt} &= -(v_{qs} - R_s i_{qs} - \omega_s \psi_{ds}) L_m / L_r L_s \alpha \\ &\quad + (v_{qr} - R_r i_{qr} - \omega_s \psi_{dr}) / L_r \alpha \end{aligned} \quad (11)$$

The stator currents  $i_{ds}$  and  $i_{qs}$  induce the subsynchronous components  $f_{er}$  into the dynamics of the rotor currents  $i_{dr}$  and  $i_{qr}$ . It should be seen that voltage dynamics and fluxes can also induce such frequencies. According to (1), on a resonance condition, the induced frequency is  $f_m = 41.67$  Hz. In this study case, it is considered the two-mass model

representation of the drive train [31] and the electrical torque can be calculated using:

$$T_e = L_m (i_{ds} i_{qr} - i_{qs} i_{dr}) \quad (12)$$

in *pu* units. The electrical torque  $T_e$  induces the oscillation in the drive train at the induced frequency  $f_m$ , according to the next equation [31]:

$$\frac{d\omega_g}{dt} = \frac{1}{2H_g} (T_m - F\omega_g - T_e) \quad (13)$$

where  $\omega_g$  oscillates at the frequency  $f_m$ . In conclusion, when the oscillation frequency of the electrical torque closely aligns with the natural frequency of the drivetrain (electromechanical mode), the system will exhibit TA.

The PMS is integrated into the APC of the BESS. This integration involves an additional reference that is selectively activated only in the presence of low-frequency oscillations, specifically those that lead to TA. The primary objective of the PMS is to isolate the two modes responsible for TA, namely the induced mode and the electromechanical mode. To achieve this goal, it is necessary to separate the subsynchronous currents in the stator from the rotor currents.

Fig. 11 shows the transformation of the signal of interest ( $i_{la}$ ,  $i_{lb}$ , and  $i_{lc}$ ), from three-phase to a  $dq$  synchronously-oriented reference frame  $\theta$ , a second-order transfer function is applied to decouple the low frequencies from the fundamental frequency. The signal  $i_{dqf}$  (i.e.,  $i_{df}$  and  $i_{qf}$ ) is the current of the fundamental frequency. The signal  $i_{dqh}$  (i.e.,  $i_{dh}$  and  $i_{qh}$ ), represents the subsynchronous components to be isolated from the generator.

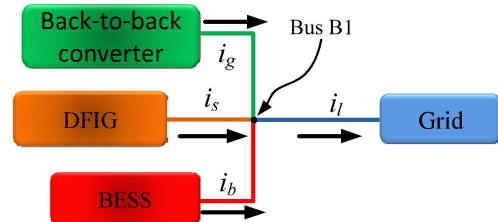


Fig. 10. Flow of the currents.

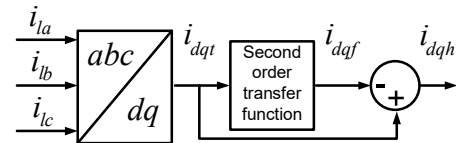


Fig. 11. Feedback currents of the PMS.

The BESS control scheme including the auxiliary signals is shown in Fig. 12, where  $i_{dh}$  and  $i_{qh}$  are inside of a blue box. The primary objective of the PMS is to provide feedback for the subsynchronous current signals to the inner loop of the BESS controller. As a result, the BESS operates as a multifunctional device capable of simultaneously mitigating TA and controlling the active power. In particular, the PMS is activated automatically only in the presence of subsynchronous current components.

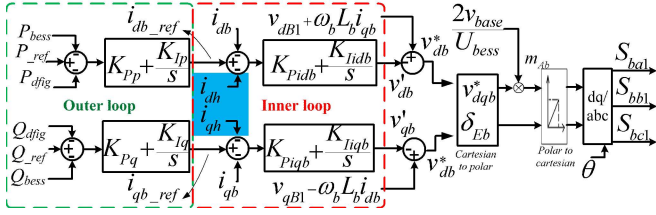


Fig. 12. BESS scheme control with the feedback currents from the PMS.

According to the  $dq$  transformation theory, the fundamental components of current  $i_{dqf}$  are constant on amplitude, and the subsynchronous components  $i_{dqh}$  oscillate. To obtain the proper feedback signals, the second-order transfer function has the objective to filtrate the fundamental signal (seen as a constant in  $dq$  reference frame) from the subsynchronous oscillation, avoiding its amplification and phase shift; the second-order transfer function is:

$$\frac{i_{dqf}}{i_{dqf}} = \frac{\omega_p^2}{s^2 + 2\zeta_p\omega_p s + \omega_p^2} \quad (14)$$

The second-order transfer function must ensure an infinite phase margin and infinite gain margin; with  $\zeta_p = 0.7$  and  $\omega_p = (4)(2)(\pi)$ , the objective can be achieved.

### B. Performance of the PMS and APC

In the preceding sections, we discussed the damping enhancement achieved by the BESS solely with APC. Specifically, the system exhibits instability at a series compensation level of 71% without the BESS. However, when the BESS is integrated with only the APC, stability is restored, and the system remains stable at a higher series compensation level up to 77.8%. It is essential to note that while this enhancement is attributed to active compensation, subsynchronous oscillations persist beyond  $K_{cs} = 77.8\%$ . Now, under the same conditions, the PMS is tested to demonstrate the outstanding results achievable with the proposed solution.

First, the SMA is conducted to show the performance of the PMS. A compensation  $K_{cs}$  from 0% to 100% is considered for three cases of study, as follows:

- The system without the BESS.
- The system with the BESS and only the APC; without the  $i_{dh}$  and  $i_{qh}$  feedback components of the inner loop in the control scheme.
- The system with the BESS and only the PMS; without the outer loop in the control scheme.

For the above cases, only the critical mode is plotted. Fig. 13 shows in a red straight line the limit where the system becomes unstable (resonance zone). The system becomes unstable without the BESS at 71% of series compensation (black line). The next case shows that when the APC is integrated into the BESS the system becomes unstable at 77.8% of series compensation (blue line). Meanwhile, the case with only the proposed mitigation scheme (green line) shows an improvement of the electromechanical mode in all spectra of series compensation, since the PMS turns the eigenvalue more

negative as the series compensation increases. These results confirm that PMS not only improves the damping of torque amplifications but also proactively prevents their occurrence. The APC, on the other hand, dampens the problem of torque amplifications only in a limited range.

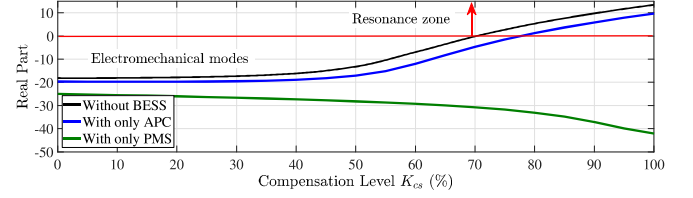


Fig. 13. Evolution of the electromechanical modes for the three cases.

Now, it is required to investigate if the APC and the PMS can operate simultaneously in the BESS. In this scenario, the system is series compensated at  $K_{cs} = 10\%$ , and two scenarios are proposed:

- The system with the BESS and only the PMS; only the inner loop.
- The system with the BESS and the PMS plus APC; included the outer-loop and the inner-loop.

At 100.3 seconds, a change of series compensation level from  $K_{cs} = 10\%$  to  $K_{cs} = 78\%$  occurs. By using the controller parameters shown in Table III and in [19], Fig. 14 shows the active power evolution through time. With only the PMS, the transient is mitigated due to the action of the proposed controller and the active power is slightly above 0.9 pu. In the scenario with the APC plus the PMS, the dynamic behavior is the same as the previous case (dynamics due to the PMS) but with the active power reaching 1 pu. The APC and the PMS achieve their objectives. In this case, it is shown that despite both schemes being applied to the BESS, the dynamics of the SSO are controlled only by the PMS and the active power compensation achieves its purpose without affecting the PMS objectives.

TABLE III  
GAINS OF THE BESS CONTROL [31]

Gain	Value	Gain	Value
$K_{Pp}$	0.1595	$K_{Ip}$	4
$K_{Pidb}$	3	$K_{Iidb}$	80
$K_{Pq}$	0.1595	$K_{Iq}$	4
$K_{Piqb}$	3	$K_{Iiqb}$	80

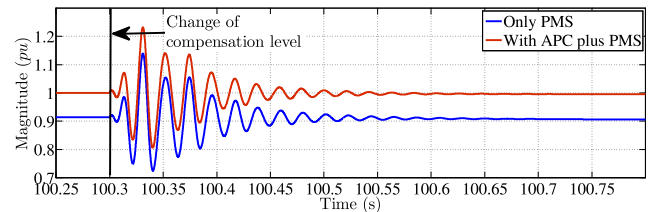


Fig. 14. Performance of the active power for the APC and the PMS.

Fig. 15 illustrates the DC voltage of the BESS converter. The scenarios align with those described for APC. Significantly, in this case, the scenarios with the PMS and the



scenario with APC plus PMS demonstrate identical dynamics, as evident from the overlap of their respective response. It is crucial to highlight that the oscillations in all state variables follow the same dynamics. This observation emphasizes the interoperability of both control schemes, suggesting their effective concurrent utilization.

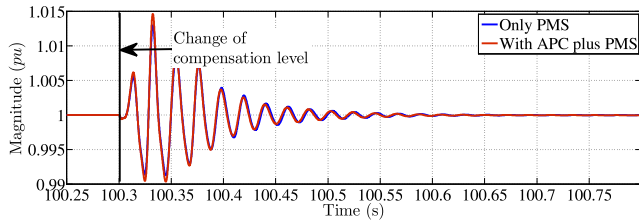


Fig. 15. Performance of the back-to-back DC voltage for the APC and the PMS.

Regarding the energy requirement by the BESS to mitigate the TA phenomenon, Fig. 16 illustrates the reactive power and the active power delivered by the BESS with only the PMS activated. Notice, that when a resonance condition is detected in the system, the powers from the BESS start to oscillate interchanging energy with the rest of the system. The results indicate that the PMS effectively damps the unstable oscillations due to the TA, ultimately leading to their disappearance with a finite amount of energy at the same series compensation.

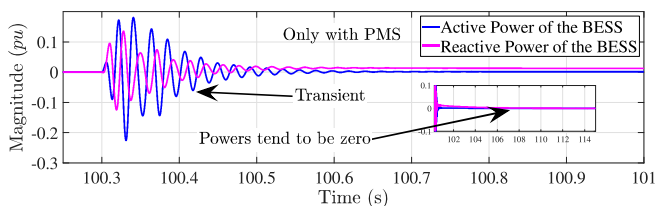


Fig. 16. Active power and reactive power delivered by the BESS with the PMS.

## VII. CONCLUSION

According to the structured process of analysis developed in this paper, it is demonstrated that it is possible to identify the physical elements related to the SSO and their natural frequency as well. This structured process entails identifying the phenomenon that produces the SSO.

Besides, it is demonstrated that, if a structured process of analysis is not used a misinterpretation of the origin of the SSO can occur, leading to a solution that partially fixes the problem.

Finally, once the phenomenon has been identified, a proposed mitigation scheme applied in the BESS is designed to mitigate the SSO with a capability of interoperability allowing the operation of the preconfigured control objectives of the BESS. The proposed mitigation scheme is activated automatically when subsynchronous currents are detected in the system. Moreover, the energy required by the proposed mitigation scheme is limited. In this context, the two physical elements that produce SSO are isolated successfully.

## APPENDIX A GAINS

The gains of the BESS control, back-to-back converter, and all model parameters, can be found in detail in [31].

## REFERENCES

- [1] D. Z. John K. Kaldellis, "The wind energy (r)evolution: A short review of a long history," *Renewable Energy*, vol. Volume 36, pp. Pages 1887–1901, 2011.
- [2] N. Verma, N. Kumar, S. Gupta, H. Malik, and F. P. García Márquez, "Review of sub-synchronous interaction in wind integrated power systems: classification, challenges, and mitigation techniques," *Protection and Control of Modern Power Systems*, vol. 8, no. 2, pp. 1–26, 2023, <https://doi.org/10.1186/s41601-023-00291-0>.
- [3] GWEC, "Wind report, global wind energy council of 2018," *Global Wind Energy Council*, April 2019.
- [4] Y. Song, E. Ebrahimzadeh, and F. Blaabjerg, "Analysis of high-frequency resonance in dfig-based offshore wind farm via long transmission cable," *IEEE Transactions on Energy Conversion*, vol. 33, no. 3, pp. 1036–1046, 2018.
- [5] L. Yang, Z. Xu, J. Østergaard, Z. Y. Dong, K. P. Wong, and X. Ma, "Oscillatory stability and eigenvalue sensitivity analysis of a dfig wind turbine system," *IEEE Transactions on Energy Conversion*, vol. 26, no. 1, pp. 328–339, 2011.
- [6] P. Kundur, J. Paserba, V. Ajjarapu, G. Andersson, A. Bose, C. Canizares, N. Hatziaargyriou, D. Hill, A. Stankovic, C. Taylor, T. Van Cutsem, and V. Vittal, "Definition and classification of power system stability IEEE/cigre joint task force on stability terms and definitions," *IEEE Transactions on Power Systems*, vol. 19, no. 3, pp. 1387–1401, 2004.
- [7] M. Amin and M. Molinas, "Understanding the origin of oscillatory phenomena observed between wind farms and hvdc systems," *IEEE Journal of Emerging and Selected Topics in Power Electronics*, vol. 5, no. 1, pp. 378–392, 2017.
- [8] H. A. Mohammadpour and E. Santi, "Analysis of subsynchronous control interactions in dfig-based wind farms: Ercot case study," in *2015 IEEE Energy Conversion Congress and Exposition (ECCE)*, 2015, pp. 500–505.
- [9] T. Ackermann, *Wind Power in Power System*. John Wiley & Sons, 2005, vol. John Wiley & Sons, Ltd.,
- [10] J. C. R. Pena and G. M. Asher, "Doubly fed induction generator using back-to-back pwm converters and its application to variable-speed wind-energy generation," in *IEE Proceedings - Electric Power Applications*, vol. 143, no. no. 3, pp. pp. 231–241, May 1996.
- [11] A. S. Trevisan, M. Fecteau, Angelo Mendonça, R. Gagnon, and J. Mahseredjian, "Analysis of low frequency interactions of dfig wind turbine systems in series compensated grids," *Electric Power Systems Research*, vol. 191, p. 106845, 2021, <https://doi.org/10.1016/j.epsr.2020.106845>.
- [12] Y. Wang, X. Jiang, X. Xie, X. Yang, and X. Xiao, "Identifying sources of subsynchronous resonance using wide-area phasor measurements," *IEEE Transactions on Power Delivery*, vol. 36, no. 5, pp. 3242–3254, 2021, <https://doi.org/10.1109/TPWRD.2020.3037289>.
- [13] Y. Zhan, X. Xie, and Y. Wang, "Impedance network model based modal observability and controllability analysis for renewable integrated power systems," *IEEE Transactions on Power Delivery*, vol. 36, no. 4, pp. 2025–2034, 2021, <https://doi.org/10.1109/TPWRD.2020.3018149>.
- [14] X. Wang, F. Blaabjerg, M. Liserre, Z. Chen, J. He, and Y. Li, "An active damper for stabilizing power-electronics-based ac systems," *IEEE Transactions on Power Electronics*, vol. 29, no. 7, pp. 3318–3329, 2014, <https://doi.org/10.1109/TPEL.2013.2278716>.
- [15] P. KUNDUR, *Power System Stability and Control*. New York: McGraw-Hill, 1994.
- [16] A. E. Leon and J. A. Solsona, "Sub-synchronous interaction damping control for dfig wind turbines," *IEEE Transactions on Power Systems*, vol. 30, no. 1, pp. 419–428, 2015.
- [17] I. J. Perez-arriaga, G. C. Verghese, and F. C. Schweppe, "Selective modal analysis with applications to electric power systems, part i: Heuristic introduction," *IEEE Transactions on Power Apparatus and Systems*, vol. PAS-101, no. 9, pp. 3117–3125, 1982, <https://doi.org/10.1109/TPAS.1982.317524>.
- [18] N. E. Costa, G. Revel, D. M. Alonso, and R. D. Fernández, "Subsynchronous control interaction studies in dfig-based wind farms using selective modal analysis," *International Journal of Electrical Power & Energy Systems*, vol. 123, p. 106291, 2020, <https://doi.org/10.1016/j.ijepes.2020.106291>. [Online]. Available: <https://www.sciencedirect.com/science/article/pii/S0142061519344175>



- [19] R. Moreno-Sánchez, C. A. Núñez-Gutiérrez, N. Visairo-Cruz, J. Hernández-Ramírez, and J. Segundo-Ramírez, "Understanding the origin of ssr in series-compensated dfig-based wind farms: Analysis techniques and tuning," *IEEE Access*, vol. 9, pp. 117 660–117 672, 2021, <https://doi.org/10.1109/ACCESS.2021.3104171>.
- [20] J. Shair, X. Xie, Y. Li, and V. Terzija, "Hardware-in-the-loop and field validation of a rotor-side subsynchronous damping controller for a series compensated dfig system," *IEEE Transactions on Power Delivery*, vol. 36, no. 2, pp. 698–709, 2021, <https://doi.org/10.1109/TPWRD.2020.2989475>.
- [21] L. Wang, X. Xie, Q. Jiang, H. Liu, Y. Li, and H. Liu, "Investigation of ssr in practical dfig-based wind farms connected to a series-compensated power system," *IEEE Transactions on Power Systems*, vol. 30, no. 5, pp. 2772–2779, 2015, <https://doi.org/10.1109/TPWRS.2014.2365197>.
- [22] M. T. Lawder, B. Suthar, P. W. C. Northrop, S. De, C. M. Hoff, O. Leitermann, M. L. Crow, S. Santhanagopalan, and V. R. Subramanian, "Battery energy storage system (bess) and battery management system (bms) for grid-scale applications," *Proceedings of the IEEE*, vol. 102, no. 6, pp. 1014–1030, 2014.
- [23] E. Reihani and R. Ghorbani, "Load commitment of distribution grid with high penetration of photovoltaics (pv) using hybrid series-parallel prediction algorithm and storage," *Electric Power Systems Research*, vol. 131, pp. 224–230, 2016, <https://doi.org/10.1016/j.epr.2015.09.004>. [Online]. Available: <https://www.sciencedirect.com/science/article/pii/S0378779615002746>
- [24] Jonmin Jo and H. Cha, "Stability of battery energy storage system operating with diesel generator in a stand-alone microgrid," in *2017 Twelfth International Conference on Ecological Vehicles and Renewable Energies (EVER)*, 2017, pp. 1–5.
- [25] Z. Yang, C. Shen, L. Zhang, M. L. Crow, and S. Atcitty, "Integration of a statcom and battery energy storage," *IEEE Transactions on Power Systems*, vol. 16, no. 2, pp. 254–260, 2001.
- [26] S. Muyeen, R. Takahashi, T. Murata, J. Tamura, and M. H. Ali, "Application of statcom/bess for wind power smoothening and hydrogen generation," *Electric Power Systems Research*, vol. 79, no. 2, pp. 365–373, 2009, <https://doi.org/10.1016/j.epr.2008.07.007>.
- [27] O. B. Adewuyi, R. Shigenobu, K. Ooya, T. Senjyu, and A. M. Howlader, "Static voltage stability improvement with battery energy storage considering optimal control of active and reactive power injection," *Electric Power Systems Research*, vol. 172, pp. 303–312, 2019, <https://doi.org/10.1016/j.epr.2019.04.004>.
- [28] J. Khazaei, A. Asrari, P. Idowu, and S. Shushekar, "Sub-synchronous resonance damping using battery energy storage system," in *2018 North American Power Symposium (NAPS)*, 2018, pp. 1–6, <https://doi.org/10.1109/NAPS.2018.8600655>.
- [29] IEEE Subsynchronous Resonance Working Group *et al.*, "Proposed terms and definitions for subsynchronous oscillations," *IEEE Transactions on Power Apparatus and Systems*, vol. PAS-99, no. 2, pp. 506–511, 1980, <https://doi.org/10.1109/TPAS.1980.319686>.
- [30] I. S. R. W. Group *et al.*, "Terms, definitions, and symbols for subsynchronous oscillations," *IEEE Transactions on Power Apparatus and Systems*, vol. PAS-104, no. 6, pp. 1326–1334, 1985, <https://doi.org/10.1109/TPAS.1985.319152>.
- [31] R. Moreno-Sánchez, "Analysis, tuning of controllers and interconnection of a battery energy storage system for subsynchronous resonance mitigation in wind farms." Ph.D. dissertation, Universidad Autónoma de San Luis Potosí, Facultad de Ingeniería, 2022. [Online]. Available: <https://repositorioinstitucional.uaslp.mx/xmlui/handle/i/8404>
- [32] N. G. Hingorani and L. Gyugyi, *Understanding FACTS: Concepts and Technology of Flexible AC Transmission Systems*. IET, 2000, pp. 425–429.
- [33] J. M. M. A. E. Leon and J. A. Solsona, "Subsynchronous resonance mitigation using variable-speed wind energy conversion systems," in *IET Generation, Transmission & Distribution*, vol. vol. 7, no. no. 5, pp. pp. 511–525, May 2013.
- [34] J. Zeng, B. Zhang, C. Mao, and Y. Wang, "Use of battery energy storage system to improve the power quality and stability of wind farms," in *2006 International Conference on Power System Technology*, 2006, pp. 1–6.
- [35] C. . L. C. . Lu and C. . Wu, "Dynamic modelling of battery energy storage system and application to power system stability," in *IEE Proceedings - Generation, Transmission and Distribution*, vol. Vol. 142, no. no. 4, pp. pp. 429–435, July 1995.
- [36] Wilsun Xu, Zhenyu Huang, Yu Cui, and Haizhen Wang, "Harmonic resonance mode analysis," *IEEE Transactions on Power Delivery*, vol. 20, no. 2, pp. 1182–1190, 2005.
- [37] M. Abdeen, M. H. Ali, A. M. A. Soliman, M. Eslami, and S. Kamel, "Improved methodology for damping sub-synchronous oscillation in a series-compensated dfig-based wind farm," *IET Generation, Transmission & Distribution*, vol. 17, no. 14, pp. 3333–3341, 2023, <https://doi.org/10.1049/gtd2.12906>.



**Roberto Moreno-Sánchez** was born in San Luis Potosí, Mexico. He received the B.S. degree in electrical-mechanical engineering in 2010, the M.Sc. degree in 2012, and the Ph.D. degree in 2022, all in electrical engineering, from the Universidad Autónoma de San Luis Potosí. He has worked in the industry performing electrical power quality analysis. His research interests include power quality, renewable energy penetration, modeling, resonance, and SSO.



**Nancy Visairo-Cruz** received a graduate degree in Electronic Engineering from the Technologic Institute of Oaxaca, México in 1997. She received the M. S. and Ph. D degrees specializing in Automatic Control from the National Center of Research and Technological Development, Cuernavaca, Mexico in 1999 and 2004, respectively. Since 2005 she has been working as a professor-researcher at the Center for Research and Graduate Studies of the Faculty of Engineering of the Autonomous University of San Luis Potosí. She is a member of the National Research System at Level 1. Among her topics of interest are automatic control schemes for power electronics systems applied to power quality, electric vehicles, renewable energy, and storage systems. She is also interested in fault diagnosis topics in energy storage systems.



**C. Alberto Núñez-Gutiérrez** received the M. Sc. and Ph. D. degrees from CENIDET, Cuernavaca in 1997, and 2002 respectively. Since 2002 he has been with the University of San Luis Potosí as a professor and researcher. He has led several research industrial projects with the mining industry, power systems industries, and government. His research interest includes power electronics, control of power converters, and power quality.



**Julio Hernández-Ramírez** received the B.Sc. degree in electrical and automation engineering in 2015, and the M.Sc. degree in electrical engineering in 2017; both from Universidad Autónoma de San Luis Potosí, San Luis Potosí, México. He worked in the National Center of Energy Control (CENACE) in Mexico City from 2018-2019 in the Electrical Studies Unit as a power system analyst. He is currently working towards a Ph.D. degree in electrical engineering at Universidad Autónoma de San Luis Potosí, San Luis Potosí, Mexico. His research

interests include modeling of renewable energy systems, stability in power systems with power electronic penetration, and electromagnetic transients.



**Juan Segundo-Ramírez** (M'10) received the M.Sc. degree from the CINVESTAV Guadalajara, Zappopan, Mexico, in 2004, and the Ph.D. degree from the Universidad Michoacana de San Nicolas de Hidalgo, Michoacán, México, in 2010, both in electrical power systems. Since 2010, he has been with the Universidad Autónoma de San Luis Potosí, San Luis Potosí, México. His research interests include power system harmonic analysis, modeling, design, and simulation.